Optical Third Harmonic Generation in Gases by a Focused Laser Beam*

J. F. Ward
The Harrison M. Randall Laboratory of Physics, The University of Michigan, Ann Arbor, Michigan 48104
and
G. H. C. New
Department of Pure and Applied Physics, The Queen's University of Belfast, N. Ireland
(Received 7 April 1969)

Optical third-harmonic generation at 2314 Å using a focused ruby laser beam (6943 Å) has been observed in a number of gases. A theory of third-harmonic generation by focused beams is presented which is used to derive atomic (or molecular) third-harmonic coefficients from the experimental data. An ambiguity in choice of a sign leads to two alternative sets of coefficients. One set is preferred on the basis of general agreement with data given in or derived from the literature: Theoretical calculations of the third-harmonic coefficients, measurements of the Kerr effect and theoretical dc hyperpolarizabilities. For helium the measured absolute value is $\chi_{He} = (7 \times 3^{\pm 1}) \times 10^{-39}$ esu/atom. For other gases the experimental values of χ in units of 10^{-39} esu/atom and scaled to $\chi_{He} = 4.0$ (a theoretical value due to Sitz and Yaris which is thought to be reliable to about 1%) are: Ne 8.9 ± 1.5; Ar 126 ± 20; Kr 386 ± 75; Xe 979 ± 150; H_2 80 ± 12; CO_2 156 ± 23; N_2 107 ± 11. Some data for $(CH_2)_2$, Cl_2, O_2, air, and glass are also presented.

I. INTRODUCTION

Optical harmonic radiation may be generated in a medium subjected to an intense light beam produced by a laser. Optical second-harmonic generation in a crystal was first demonstrated by Franken and co-workers[1] and third-harmonic generation in crystals, glasses, and liquids was subsequently reported by Maker, Terhune, and Savage.[2] We have detected and measured third harmonic radiation at 2314 Å generated in a number of gases by a focused ruby laser beam (6943 Å).

The gases studied were helium, neon, argon, xenon, krypton, molecular hydrogen, carbon dioxide, nitrogen, oxygen, ethylene, chlorine, and air. Some of the results were presented previously in a brief report.[3] The experiments are described in Sec. II.

The propagation of harmonic radiation generated by a focused light beam in an isotropic medium is investigated in Sec. III. This theory is used to derive atomic (or molecular) coefficients from the experimental data.

Gases have been studied in this work because of the relative ease with which calculations may be performed for an isolated atom (or molecule). This applies both to *ab initio* quantum-mechanical calculations of the third-harmonic coefficients and to less sophisticated calculations which relate the coefficients for different nonlinear processes. In Sec. IV, experimental third-harmonic coefficients are compared with various theoretical results and values derived from measurements of the Kerr effect and calculations of the dc hyperpolarizability.

II. EXPERIMENTAL

A schematic diagram of the apparatus is shown in Fig. 1. A rotating prism Q-switched ruby laser (Lear-Siegler LS 100) provided a plane polarized fundamental light beam at 6943 Å. The leading pulse was 30 nsec wide at half-height with 1–3 MW peak power: Subsequent smaller pulses were also present. The signal from a photocell (RCA 922) monitoring the fundamental light was displayed on one beam of a dual-beam oscilloscope (Tektronix Type 551 with type L preamplifiers). The laser beam passed through a red filter (Chance OR1) to attenuate stray flash-tube light and was focused by a 15-cm lens 3 cm in front of the $\frac{1}{8}$-in.-thick glass entrance window of a cell containing the gas under observation at pressures in the range 0–6 atm. All succeeding optical components were made of

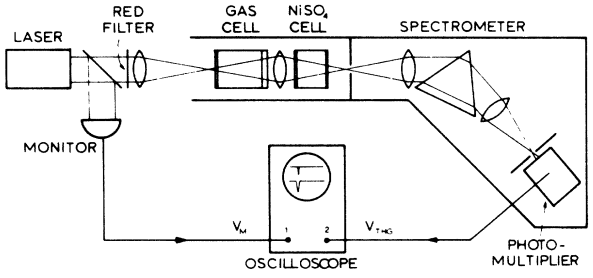

FIG. 1. Schematic diagram of the apparatus.

quartz to pass the ultraviolet third-harmonic radiation (2314 Å). This choice of windows in the gas cell and their positioning with respect to the focused laser beam will be discussed in Sec. III. Almost all the fundamental light was absorbed in a $3\frac{1}{2}$-cm cell containing saturated aqueous $NiSO_4$ solution, and further wavelength discrimination was effected with a prism spectrometer having a resolution of 200 Å. The signal from the photomultiplier detector (Mazda 27M3), corresponding typically to 50 photoelectrons at the photocathode or about 10^4 third-harmonic photons originally generated, was displayed on the other beam of the oscilloscope and photographed together with the trace from the monitor photocell. A typical oscilloscope trace is shown in Fig. 2. The pulse heights V_{THG} and V_M are proportional to the peak power at 2314 Å ($\mathcal{P}^{3\omega_1}$) and 6943 Å ($\mathcal{P}^{\omega_1}$), respectively.

The oscilloscope traces exhibited all the characteristic features of third harmonic radiation. A log-log plot of $\mathcal{P}^{3\omega_1}$ versus $\mathcal{P}^{\omega_1}$ is shown in Fig. 3 for 28 shots of varying power in an otherwise unchanged experimental situation. The third-harmonic power is expected to vary as the cube of the fundamental power

$$\mathcal{P}^{3\omega_1} \propto (\mathcal{P}^{\omega_1})^3 . \qquad \text{(II. 1)}$$

The points in the figure are correspondingly scattered about a line of slope 3. The error bars were estimated on the basis of the statistical errors in the detection of the small number of third-harmonic photons. Additional data scatter may arise from variation in the laser mode structure. A further prediction from the cubic relationship of Eq. (II. 1) is that the harmonic pulse should be narrower than the fundamental. This feature is apparent in Fig. 2; the measured pulse widths are consistent with theory when allowance is made for the 16 nsec rise time of the detector.

Third-harmonic power increased as the distance of the glass window from the focus was reduced (see Sec. III). It was, however, necessary to make this distance large enough so that spurious signals, due to laser induced breakdown of the window, did not occur. Mild breakdown was found to produce a pulse with time dependence similar to that of the fundamental and did not do any visible damage to the window. Such signals are distinguished from third harmonic by their broad spectral distribution and irregular amplitude.

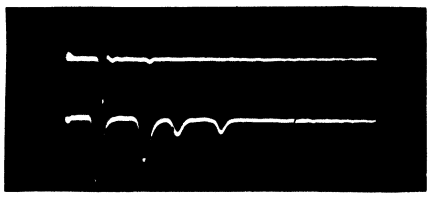

FIG. 2. Double-beam oscilloscope trace of third-harmonic (upper) and fundamental monitor (lower) signals. The cubic dependence of $\mathcal{P}^{3\omega 1}$ on $\mathcal{P}^{\omega 1}$ not only affects the relative pulse heights in each channel but also causes the harmonic pulses to be narrower than the fundamental pulses.

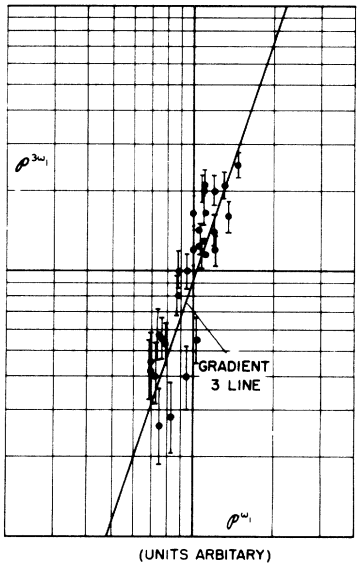

FIG. 3. Dependence of $\mathcal{P}^{3\omega_1}$ on $\mathcal{P}^{\omega_1}$ plotted on a log-log scale for 28 shots in a given experimental situation. The error bars reflect the statistical error in the detection of a small number of third-harmonic photons.

A final interesting check on the nature of the signal is its dependence on the fundamental polarization. For an isotropic nonlinear medium, a plane-polarized fundamental generates a similarly polarized third harmonic but circularly polarized fundamental does not generate harmonics.[4] Physically this may be understood as follows: The electric field vector for a circularly polarized fundamental wave rotates in space at the fundamental frequency and is constant in amplitude throughout the optical cycle. The polarization vector rotates parallel to the electric field vector in an isotropic medium and the amplitude is constant even though it is not linearly related to the fundamental field amplitude. Thus the polarization has no harmonic content. We used a z-cut potassium dihydrogen phosphate crystal as a voltage-dependent retardation plate to vary the polarization of the fundamental and observed the total harmonic intensity (see Fig. 4). This is seen to be in agreement with the above prediction.

Each laser pulse yields a relative value for S,

$$\text{where} \qquad S \equiv \mathcal{P}^{3\omega_1}/(\mathcal{P}^{\omega_1})^3 \propto V_{THG}/V_M^{\,3} . \qquad \text{(II. 2)}$$

S is shown in Fig. 5 plotted for various gases as a function of pressure. The form of these curves

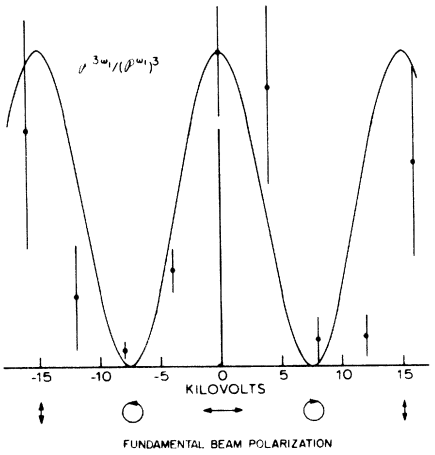

FIG. 4. Third-harmonic signal as a function of the voltage applied to a potassium dihydrogen phosphate electro-optic retardation plate. The voltage necessary to produce minimum signal is greater than the quarter wave voltage owing to the particular electrode configuration employed.

is derived in Sec. III and nonlinear coefficients extracted and compared with other data in Sec. IV.

III. HARMONIC GENERATION BY A FOCUSED LASER BEAM

Second-harmonic generation by focused laser beams has been discussed by several authors.[5-7] Although the primary concern of this paper is with third-harmonic generation, the general qth-harmonic case is analyzed in order to facilitate comparison with second-harmonic results. The analysis is confined to isotropic nonlinear media but otherwise follows closely that applied by Kleinman *et al.*[6] to second-harmonic generation.

The fundamental laser beam is assumed to be focused inside a homogeneous, isotropic, nonlinear medium occupying the half-space $z>0$, the other half-space being empty. Depletion of the fundamental power by the nonlinear process is neglected. The simplest field distribution in the focused beam is a lower-order Gaussian mode:

$$\vec{E}_1(\vec{r},\ t)=\tfrac{1}{2}\{\vec{E}_1(\vec{r})e^{-iw_1t}+\vec{E}_1{}^*(\vec{r})e^{+iw_1t}\}\ , \quad \text{(III. 1)}$$

where

$$\vec{E}_1(\vec{r})=\vec{E}_0e^{ik_1z}(1+i\xi)^{-1}$$

$$\times\exp[-k(x^2+y^2)/b(1+i\xi)]\ . \quad \text{(III. 2)}$$

The extension of the theory to the situation where the beam has a more complicated structure will be discussed briefly at the end of this section. In Eq. (III. 2), k_1 is the fundamental wave vector; b is the confocal parameter for the mode, related to δ_1, the far field semiangular spread of the beam by

$$b=4/\delta_1{}^2k_1\ ; \quad \text{(III. 3)}$$

E_0 is the electric field amplitude at the center of the focal spot, and ξ is a normalized z coordinate related to the position of the focus at $z=f$ by

$$\xi=2(z-f)/b\ . \quad \text{(III. 4)}$$

A complete list of symbols is given at the end of this section and the meaning of some of them is clarified in Fig. 6.

An important feature of Eq. (III. 2) is the factor $(1+i\xi)^{-1}$ which may be rewritten

$$(1+i\xi)^{-1}=(1+\xi^2)^{-1/2}\exp(-\tan^{-1}\xi)\ . \quad \text{(III. 5)}$$

$(1+\xi^2)$ is proportional to the beam area A. The field distribution thus exhibits a field strength which varies as $A^{-1/2}$ and a phase variation additional to $\exp(ik_1r)$ which increases from 0 at the center of the focal spot to $\mp\pi/2$ as ξ (or z) becomes equal to $\pm\infty$.

The qth-harmonic polarization of the medium $\vec{P}^{(q)}(\vec{r},t)$ with frequency $\omega=q\omega_1$ is:

$$\vec{P}^{(q)}(\vec{r},\ t)=\tfrac{1}{2}\{\vec{P}^{(q)}(\vec{r})e^{-i\omega t}+\vec{P}^{(q)*}(\vec{r})e^{+i\omega t}\}\ , \quad \text{(III. 6)}$$

where $\vec{P}^{(q)}(\vec{r})$ is related to the fundamental electric field by the qth-order tensor susceptibility $\underline{\underline{X}}(-\omega;\ \omega_1,\ \omega_1\ldots)$

$$\vec{P}^{(q)}(\vec{r})=2^{(1-q)}\underline{\underline{X}}(-\omega;\ \omega_1,\ \omega_1\ldots)[\vec{E}_1(\vec{r})]^q\ . \quad \text{(III. 7)}$$

The definition and notation used here for the nonlinear coefficients is discussed in Appendix A. It is convenient for the rest of this section to abbre-

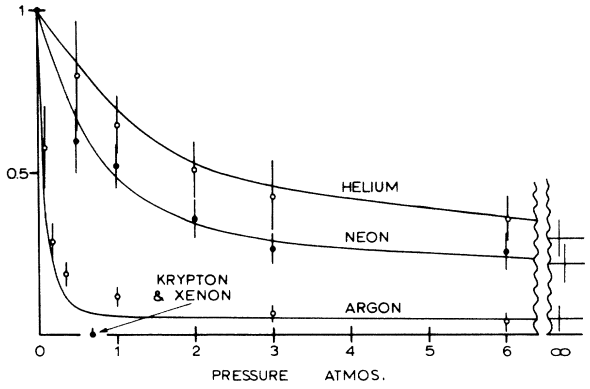

FIG. 5. Third-harmonic signal as a function of pressure for five inert gases. The solid curves were calculated theoretically and fitted to the experimental points.

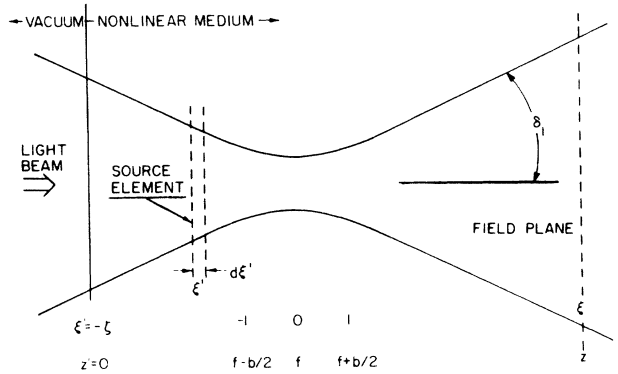

FIG. 6. Notation for harmonic generation by a lowest-order Gaussian beam.

viate $\underline{X}(-\omega;\omega_1,\omega_1\ldots)$ to $\underline{X}^{(q)}$ and to consider only one component of Eq. (III. 7) omitting the tensor notation. Substitution of Eq. (III. 2) into Eq. (III. 7) yields

$$P^{(q)}(\vec{r}) = 2^{(1-q)}X^{(q)}E_0{}^q \exp(ik'z) \times(1+i\xi)^{-q}\exp\left(-\frac{k'(x^2+y^2)}{b(1+i\xi)}\right)B(z)\ , \qquad \text{(III. 8)}$$

where $k' = qk_1$ (III. 9)

$$\omega = q\omega_1 \qquad \text{(III. 10)}$$

$$B(z)=1, \quad (z>0) \qquad =0, \quad (z<0)\ . \qquad \text{(III. 11)}$$

$P_{\vec{K}}^{(q)}$, the component of the harmonic polarization with wave vector $\vec{K}$, is obtained by Fourier decomposition of $P^{(q)}(\vec{r})$.

$$P_{\vec{K}}^{(q)} = (2\pi)^{-3}\int_{-\infty}^{-\infty} P^{(q)}(\vec{r}'')\exp(-i\vec{K}\cdot\vec{r}'')d\vec{r}''\ . \qquad \text{(III. 12)}$$

The harmonic electric field arising from this polarization component is [8]

$$E_{\vec{K}}(\vec{r}) = -[2\pi k_0{}^2 P_{\vec{K}}^{(q)} z/k]g(U_{\vec{K}})\exp(i\vec{K}\cdot\vec{r})\ , \qquad \text{(III. 13)}$$

where k is the wavevector for a free-harmonic wave in the medium, k_0 is the wave vector for a harmonic wave in free space,

$$U_{\vec{K}} = i\{K_z - k' + (K_x{}^2+K_y{}^2)/2k' + \Delta k\} \qquad \text{(III. 14)}$$

and $$g(x) = (1-e^{-x})/x = \int^1 e^{-xp}dp\ . \qquad \text{(III. 15)}$$

In the derivation of Eq. (III. 13), it has been assumed that the angular spread of the fundamental beam is small, and the nominal mismatch Δk is small

$$\Delta k = k' - k,\ |\Delta k| \ll k', k\ . \qquad \text{(III. 16)}$$

Equation (III. 13) may be recast in the form

$$E_{\vec{K}}(\vec{r}) = -(i\pi k_0{}^2 b/k)\int_{-\zeta}^{\xi} P_{\vec{K}}^{(q)} \times\exp[\tfrac{1}{2}U_{\vec{K}}b(\xi'-\xi'')]\exp(i\vec{K}\cdot\vec{r})d\xi'\ , \qquad \text{(III. 17)}$$

where $-\zeta$ is $-2f/b$ which is the location of the vacuum-medium interface.

The total harmonic electric field can now be obtained by combining this equation with Eqs. (III. 8) and (III. 12) and integrating over $d\vec{K}$. The integration over dK_z gives $\delta(z'-z'')$ so that $B(z'')$ from Eq. (III. 8) may be replaced by $B(z')$ which can then be ignored since it is unity in the range of the integration over $d\xi'$. After integrating over dz'' the integrations over dx'', dy'', dK_x, dK_y may be done in any order yielding finally

$$E(\vec{r}) = [i2^{(1-q)}\pi k_0{}^2 b X^{(q)}E_0{}^q/k]\exp(ik'z)(1+i\xi)^{-1} \times\exp\left(\frac{-k'(x^2+y^2)}{b(1+i\xi)}\right)I(q,\Delta k,\xi,\zeta)\ , \qquad \text{(III. 18)}$$

where

$$I(q,\Delta k,\xi,\zeta) \equiv \int_{-\zeta}^{\xi} d\xi' \frac{\exp[\frac{1}{2}ib\Delta k(\xi'-\xi)]}{(1+i\xi')^{q-1}}\ . \qquad \text{(III. 19)}$$

This harmonic field is a lowest-order Gaussian mode (this depends, of course, on our choice of fundamental mode) having the same confocal parameter b as the fundamental beam and therefore smaller angular divergence. The amplitude of the field is governed by the remaining integral $d\xi'$ (or dz') which must be carried out explicitly for each experimental situation.

The integral I can be evaluated analytically for an infinite medium ($\xi,\zeta\to\infty$) in which case:

$$\int_{-\infty}^{\infty} d\xi' \frac{\exp(\frac{1}{2}ib\Delta k\xi')}{(1+i\xi')^{q-1}} = 0\ , \qquad \Delta k<0$$

$$= \frac{2\pi}{(q-2)!}(b\Delta k/2)^{q-2}\exp(-b\Delta k/2)\ , \quad \Delta k>0 \qquad \text{(III. 20)}$$

for $q=2$, (second-harmonic generation) this yields

$$I(2,\Delta k,\infty,\infty) = 0, \quad \Delta k<0 \qquad = \pi, \quad \Delta k=0 \qquad = 2\pi\exp(-\tfrac{1}{2}b\Delta k), \quad \Delta k>0 \qquad \text{(III. 21)}$$

and for $q = 3$, (third-harmonic generation)

$$I(3, \Delta k, \infty, \infty) = 0, \qquad \Delta k \leq 0$$
$$= \pi b \Delta k \exp(-\tfrac{1}{2} b \Delta k), \qquad \Delta k > 0 . \tag{III. 22}$$

The interesting feature emerges that no third harmonic is generated by focusing in an infinite medium at nominal phase matching ($\Delta k = 0$).

If absorption occurs for the fundamental and harmonic, Eqs. (III. 18) and (III. 19) [but not Eqs. (III.20), (III.21), and (III.22)] still apply. In this case the wave vectors in Eqs. (III. 18) and (III. 19) are complex and depend on α_1 and α, the intensity absorption coefficients at ω_1 and ω, respectively,

$$\begin{aligned} &\mathrm{Im}(k_1) = \tfrac{1}{2}\alpha_1 , \\ &\mathrm{Im}(k') = \tfrac{1}{2} q \alpha_1 , \\ &\mathrm{Im}(k) = \tfrac{1}{2}\alpha , \\ &\mathrm{Im}(\Delta k) = \tfrac{1}{2} q \alpha_1 - \tfrac{1}{2}\alpha . \end{aligned} \tag{III. 23}$$

The conclusions of this section remain essentially unchanged when higher-order modes of the fundamental beam are present. There is no difficulty in principle in analyzing this situation although the algebra becomes progressively more involved the more complicated are the modes considered. The harmonic field can always be expressed as a linear combination of terms, the leading terms being of the form given in Eq. (III. 19) and further terms having higher powers of $(1 + i\xi')$ in the denominator.

For convenience we reidentify here some of the notations used in this section:

$\vec{E}_1(\vec{r}, t), \vec{E}_1(\vec{r})$	fundamental electric field
$\vec{E}_0$	maximum fundamental electric field
$\vec{P}^{(q)}(\vec{r}, t), \vec{P}^{(q)}(\vec{r})$	harmonic polarization
$\vec{E}(\vec{r})$	harmonic electric field
q	harmonic number
ω_1	fundamental angular frequency
$\omega = q\omega_1$	harmonic angular frequency
k_1	fundamental wave vector in the medium
$k' = qk_1$	harmonic forced wave vector in the medium
k	harmonic free wave vector in the medium
k_0	harmonic free wave vector in the vacuum
K	wave vector for a component of the harmonic polarization
$\Delta k = qk_1 - k$	wave-vector mismatch
z	coordinate along the direction of propagation of the beam
f	z coordinate of the focus
b	confocal parameter Eq. (III. 3).
δ_1	far field semiangular spread of the fundamental beam
ξ	normalized z coordinate Eq. (III. 4).

Vibration Curves

The integral I may be evaluated for each experimental configuration either numerically or by analytical approximation. We have found it helpful to consider, in addition, a graphical interpretation which we first illustrate for the case of harmonic generation by a plane-wave fundamental beam. The harmonic field expressed in terms of an integral analogous to I is

$$E(\vec{r}) \propto iX \int_0^z \exp[i\Delta k(z' - z)]\, dz' . \tag{III. 24}$$

The contribution from each element dz' is represented in amplitude and phase by an infinitesimal vector in the complex plane. The curve traced out by adding the infinitesimal vectors may be called a vibration curve.[9, 10] The integral of Eq. (III. 24) corresponds to the section of the curve from $z' = 0$ to $z' = z$ or equivalently to the resultant vector joining those points.

In the index matched situation ($\Delta k = 0$), the vibration diagram is simply a straight line as shown in Fig. 7(a). For a transparent mismatched medium (Δk real and nonzero), the vibration curve is circular in shape. Figure 7(b) illustrates this for a sample with Δk negative and length l_c called the coherence length.

$$l_c = \pi / \Delta k . \tag{III. 25}$$

As the sample length is increased, the circle is repeatedly retraced by the tail of the vibration curve, the resultant harmonic field being a maximum whenever z is an odd multiple of l_c. It is important to notice that for $\Delta k \neq 0$, the maximum value of the field, determined by the diameter of the circle, is proportional to $X^{(q)}/\Delta k$ rather than $X^{(q)}$ alone. When, in addition to being mismatched

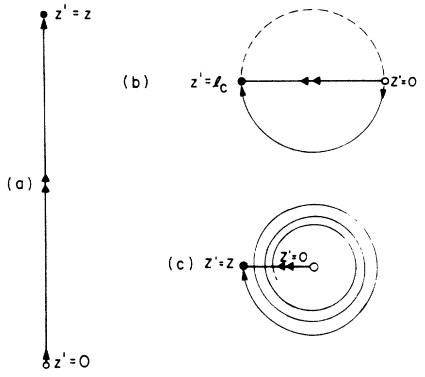

FIG. 7. Vibration diagrams for harmonic generation by a plane-wave fundamental. The fundamental beam enters the nonlinear medium at $z'=0$. The vibration curve is indicated by single arrows, and the vector representing the resultant harmonic field at $z'=z$ is indicated by a double arrow. (a) Index matching $\Delta k=0$ (b) index mismatch, $\Delta k<0$. The vibration curve is shown for sample length equal to a coherence length. As the length of the sample is increased the tail of the vibration curve repeatedly retraces the circle. (c) Index mismatched and with mild absorption at the harmonic. The spiral has been drawn for $\mathrm{Im}(\Delta k)$ equal to $|\Delta k|/(10\pi)$.

the sample is also mildly absorbing to the harmonic radiation $[0<\mathrm{Im}(\Delta k)\ll|\Delta k|]$, the circle becomes a spiral. Figure 7(c) shows the vibration curve for a thick sample with $\mathrm{Im}(\Delta k)$ chosen to be $\Delta k/(10\pi)$, the center of the spiral being omitted for clarity. The magnitude of the resultant field for a sample substantially longer than the absorption length is now half that of Fig. 7(b) and is independent of the small absorption coefficient and the thickness.

For a focused fundamental beam the vibration curve represents the integral I of Eq. (III. 19) rather than Eq. (III. 24). The difference (apart from the convenient use of the normalized coordinate ξ rather than z) is that the integral I includes an additional factor $(1+i\xi')^{1-q}$. This may be rewritten

$$(1+i\xi')^{1-q}=a_q(\xi')\exp[i\phi_q(\xi')]\ , \quad \text{(III. 26)}$$

where

$$a_q(\xi')=(1+\xi'^2)^{-(q-1)/2}=[A(\xi')]^{-(q-1)/2}\ , \quad \text{(III. 27)}$$

and

$$\phi_q(\xi')=-(q-1)\tan^{-1}\xi'\ , \quad \text{(III. 28)}$$

to emphasize that the effect of focusing is to weight, both in amplitude and in phase, the contribution of the element $d\xi'$ to the harmonic field.

We digress briefly to show that Eqs. (III. 27) and (III. 28) are in accord with the results of more intuitive arguments. Focusing contributes $\tan^{-1}\xi'$ to the phase of the fundamental field [Eq. (III. 5)] and consequently $\tan^{-1}\xi'$ and $q\tan^{-1}\xi'$ to the phases of the fundamental and harmonic polarizations, respectively. The fundamental polarization is ideally phased to reradiate into the focused mode. The misphasing of the harmonic polarization due to focusing is therefore its phase with respect to the fundamental polarization, which is correctly accounted for by $\phi_q(\xi')$. The function $a_q(\xi')$ is the relative amplitude at ξ of the harmonic field contributions arising from elements $d\xi'$ at ξ'. The fundamental power is independent of ξ' so that the fundamental field goes as $[A(\xi')]^{-1/2}$ where $A(\xi')$ is the beam area at ξ'. The harmonic polarization and therefore the harmonic field contribution at $\xi'+d\xi'$ is proportional to the qth power of the fundamental field $[A(\xi')]^{-q/2}$. The harmonic power at $\xi'+d\xi'$ is proportional to $A(\xi')\times$ harmonic field squared, i.e., $[A(\xi')]^{1-q}$. At ξ this power is spread over an area independent of ξ' so that the field contribution goes as the square root of the power, i.e., $[A(\xi')]^{(1-q)/2}$ which is correctly accounted for by $a_q(\xi')$.

Vibration curves for second and third harmonic generation by a focused beam in a transparent medium at nominal index matching ($\Delta k=0$) are shown in Fig. 8. The shape of the curves is seen to be consistent with the requirement of Eq. (III. 28) that the phase of contributions changes by $\mp(q-1)\pi/2$ from the focus to $\xi'=\pm\infty$. For second harmonic generation [Fig. 8(a)] the $\xi'=\pm\infty$ points have a finite separation, but are both infinitely far from the $\xi'=0$ point (the focus). The resultant field generated in an infinite medium is repre-

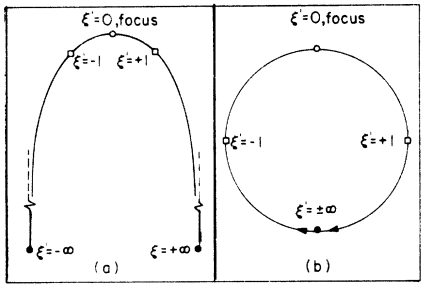

FIG. 8. Vibration curves for harmonic generation by a focused fundamental beam in the index matched case $\Delta k=0$. (a) Second harmonic (b) third harmonic. The resultant harmonic field for an infinite medium is represented by a vector joining the points $\xi'=-\infty$ to $\xi'=+\infty$. This is finite for second harmonic but is zero for third harmonic since the two points are coincident.

sented by the vector joining $\xi'=-\infty$ to $\xi'=+\infty$ and is finite. A much larger resultant is obtained joining points ξ' small to ξ' large corresponding to a long crystal with the focus near one surface.[7] For index matched third harmonic [Fig. 8(b)] the points $\xi'=-\infty$ and $\xi'=+\infty$ coincide so that no net harmonic is generated in an infinite medium. The total length of the second-harmonic vibration curve is infinite when the range of ξ' is $\pm\infty$, but the third-harmonic curve has a finite length. In both cases the length is independent of Δk, which affects only the curvature ρ^{-1} of the vibration diagrams.

$$\rho^{-1}=[(1+\xi'^2)b\Delta k/2-(q-1)](1+\xi'^2)^{(q-3)/2}. \quad \text{(III. 29)}$$

Figure 9 shows vibration curves for varying degrees of index mismatch ($-0.3<b\Delta k<+2.0$) with $X^{(q)}$ held constant. Only half of each curve is shown ($\xi'>0$) from which the other half ($\xi'<0$) may be obtained by reflection in a vertical line through $\xi'=0$. It is evident that the sense of the curvature contributed by the mismatch depends on the sign of Δk. Negative Δk accentuates and positive Δk tends to compensate the curvature present with Δk zero. An infinite medium having negative Δk yields no net second or third harmonic. However, for Δk positive, there exists an optimum value of the mismatch which yields maximum harmonic generation. In an infinite medium, optimum second harmonic generation takes place with an infinitesimally positive value of Δk in which case the $\xi'=+\infty$ point lies on the dashed line drawn in Fig. 9(a). The resultant harmonic field is twice that for

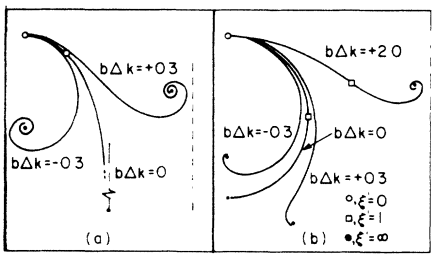

FIG. 9. Vibration curves for harmonic generation by a focused fundamental beam with various values of $b\Delta k$ with $\chi^{(q)}$ constant: (a) Second harmonic (b) third harmonic. The index matched curves $b\Delta k=0$ are repeated here from Fig. 8. The region $\xi'>0$ is shown, the other half-region being obtained by reflection in the vertical line through $\xi'=0$. The asymmetry with sign of $b\Delta k$ is evident. The optimum value of $b\Delta k$ for second harmonic in an infinite medium is positive infinite-simal and the $\xi'=+\infty$ point then lies on the dashed vertical line: for third harmonic $b\Delta k=+2$ is optimum.

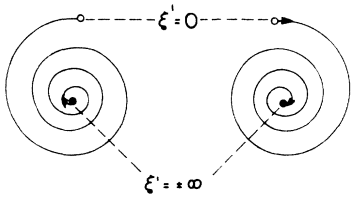

FIG. 10. Schematic vibration curve for second or third harmonic generation by a focused fundamental beam with $b\Delta k$ large negative. The contributions to the field from regions on either side of the focus have been separated for clarity. A curve for $b\Delta k$ large positive can be obtained by reflection in the horizontal line through $\xi'=0$. The scale of the curves for constant $X^{(q)}$ goes as $(b\Delta k)^{-1}$ while the shape is unchanged. Δk may be varied in a gaseous nonlinear medium by changing the pressure but in this case $X^{(q)}/\Delta k$ remains constant so that the form and scale of the vibration curve is independent of pressure so long as Δk is large.

$\Delta k=0$. This result may also be derived analytically from Eq. (III. 19). In the equivalent case for third harmonic generation, $\Delta k_{\text{optimum}}$ is $+2/b$ [see Fig. 9(b)].

The advantage of positive Δk may be understood from a physical point of view. Positive Δk means $|k|<q|k_1|$, but wave-vector match can still be achieved for noncollinear plane-wave components existing within the focused fundamental beam. For example, at optimum matching for third harmonic generation in an infinite medium, wave vectors for three fundamental beam components inclined at angles to the beam direction $-\delta_1, 0, +\delta_1$ are matched to a harmonic wave vector in the beam direction.

When Δk is very large ($b\Delta k\gg 1$) the curvature of the vibration diagram [see Eq. (III. 29)] is large and proportional to Δk. The form of the curve is then independent of the sign of Δk and becomes a tight spiral having the $\xi'=\pm\infty$ points coincident for both second and third harmonic. This is shown schematically in Fig. 10. The scale of the diagram is determined by the ratio of the length to the curvature, $X^{(q)}/\Delta k$ which for a given medium is independent of density. This situation is discussed further in the following section.

Experimental Configuration

The experimental arrangement in the region of the focus is shown in Fig. 11(a). A solid nonlinear medium S transparent to the fundamental radiation separates the two regions G and G' occupied by gas. The simplified configuration of Fig. 11(b) is studied first and later shown to be equivalent to the experimental one when the solid is absorbing to the third harmonic radiation. In Fig. 11(b), the solid occupies the region S ($-\infty<\xi'<\xi_I$) and the gas under observation the region G ($\xi_I<\xi'<\xi_D$).[11] The plane ξ_D is effectively at infinity in the sense that

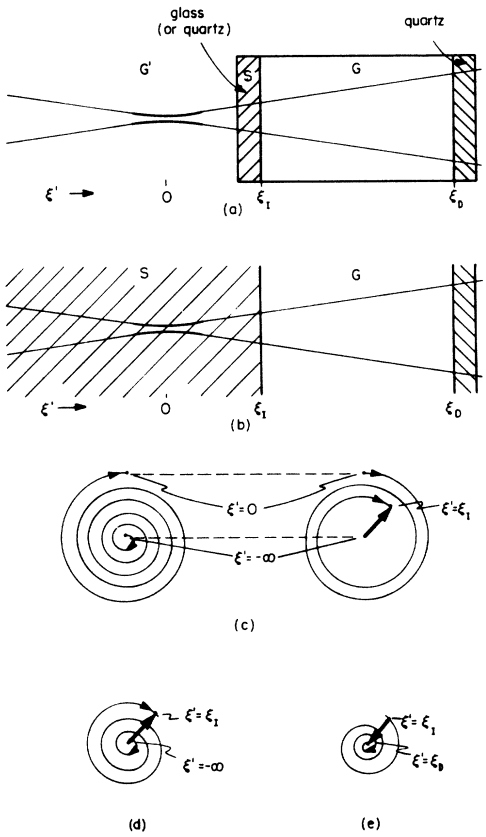

FIG. 11. (a) Experimental configuration in the region of the focus. The plane ξ_D is sufficiently far from the focus that no third harmonic radiation is generated in the quartz exit window of the gas cell. (b) The simplified configuration studied in the text. It is shown in the text to be equivalent to (a) when the solid medium S absorbs the third harmonic radiation. (c) Schematic vibration curve representing the harmonic field generated by the solid [E_S of Eq. (III.39)] for the arrangement shown in (b). The contributions to the field from the regions on either side of the focal point have been separated for clarity. (d) Vibration curve as in (c) except that the solid medium is mildly absorbing at the third harmonic wavelength. The amplitude and phase of E_S are essentially the same in the two cases provided that there is negligible absorption in one coherence length. This vibration curve also applies to the experimental arrangement (a) provided that the thickness of the glass window is very much larger than a harmonic absorption length. (e) Vibration curve representation of the harmonic field for a gas at high pressure [E_G of Eq. (III.48)]. The total harmonic field when region G is filled with gas at high pressure is the vector sum of the solid and gas contributions shown in (d) and (e), respectively. These contributions are in antiphase and cancel if $(X/\Delta k)_G = (\eta/\Delta k)_S$.

the fundamental beam has expanded sufficiently for no significant third harmonic generation to take place for $\xi' > \xi_D$.

The experimentally determined quantity is S the ratio of the third-harmonic power $\mathcal{P}^{\omega}$ to the cube of the fundamental power $\mathcal{P}^{\omega_1}$, both measured at the plane ξ_D as a function of the pressure of the gas in region G:

$$S = \mathcal{P}^{\omega}/(\mathcal{P}^{\omega_1})^3 . \tag{III. 30}$$

An expression is required relating the signal S to the third-harmonic coefficients.

A lowest-order Gaussian mode as in Eq. (III. 2) is taken for the fundamental beam propagating from the solid (S) through the interface (I) to the gas (G).

$$E_1(\vec{r}) = (E_0/T_1)\exp(ik_{1S}z) \times \mathcal{G}(x, y, \xi_S, k_{1G}/b_G); \quad z < z_I, \quad \xi_S < \xi_I$$

$$E_1(\vec{r}) = E_0 \exp[ik_{1S}z_I + ik_{1G}(z - z_I)] \times \mathcal{G}(x, y, \xi_G, k_{1G}/b_G); \quad z > z_I, \quad \xi_G > \xi_I , \tag{III. 31}$$

where the Gaussian beam shape is given by

$$\mathcal{G}(x, y, \xi, k/b) = (1 + i\xi)^{-1} \exp\left(-\frac{k(x^2 + y^2)}{b(1 + i\xi)}\right). \tag{III. 32}$$

T_1 is the transmission coefficient for the fundamental at the interface

$$T_1 = 2k_{1G}/(k_{1G} + k_{1S}) . \tag{III. 33}$$

The ξ scale which depends on b [see Eq. (III. 4)] changes at the interface but is continuous

$$\xi_{SI} = \xi_{GI} = \xi_I . \tag{III. 34}$$

Use has been made in Eq. (III. 31) of the relation

$$k_S/b_S = k_G/b_G , \tag{III. 35}$$

which expresses Snell's law for the refraction of the beam at the interface.

Equations (III. 2) and (III. 18) constitute a relation between fundamental and harmonic fields. Applied to Eq. (III. 31), this yields an expression for $E_S(x, y, \xi_{I-})$, the harmonic field generated in the solid, evaluated just before the interface.

$$E_S(x, y, \xi_{I-}) = \frac{i\pi k_0^2 b_S}{4k_S} X_S \left(\frac{E_0}{T_1}\right)^3 \exp(ik_S' z_I)$$

$$\times \mathcal{G}(x, y, \xi_I, k_S'/b_S) I_S \ , \qquad \text{(III. 36)}$$

where

$$I_S = \int_{-\infty}^{\xi} I d\xi_S' \frac{\exp[ib_S \Delta k_S (\xi_S' - \xi_I)/2]}{(1 + i\xi_S')^2} \ . \qquad \text{(III. 37)}$$

Integration by parts yields an asymptotic expansion in $(b_S \Delta k_S)^{-1}$ and if $b_S \Delta k_S \gg 1$ it is satisfactory to discard all but the leading term. This condition is satisfied in the experimental situation and implies that the beam area changes insignificantly within a coherence length. Thus,

$$I_S = [ib_S \Delta k_S (1 + i\xi_I)^2/2]^{-1} \ . \qquad \text{(III. 38)}$$

With this approximation the harmonic generated in the solid, evaluated at the detector plane ξ_D is

$$E_S(x, y, \xi_D) = \eta \frac{X_S}{\Delta k_S} \frac{\pi k_0}{2} (1 + i\xi_I)^{-2} E_0^3 \times \exp[ik_S' z_I + ik_G (z_D - z_I)] \times \mathcal{G}(x, y, \xi_D, k_0/b_G) \ , \qquad \text{(III. 39)}$$

where refractive indices for the gas have been set to unity except in the phase and in Δk_G. The factor η includes a coefficient T for transmission of the harmonic at the interface, analogous to T_1 of Eq. (III. 33) and is given by

$$\eta = \frac{k_0}{k_S} \frac{T}{T_1^3} = \frac{2k_0}{k_0 + k_S} \left(\frac{k_0/3 + k_{1S}}{2k_{1S}} \right)^3 \ . \qquad \text{(III. 40)}$$

If the refractive index of the solid at fundamental and harmonic is taken to be 1.5 then η is approximately $\frac{1}{2}$. Knowledge of the magnitude of η is not relevant to the extraction of third-harmonic coefficients for gases from the experimental data.

The field in the region G is related to the power by

$$\mathcal{P} = \frac{c}{8\pi} \int\int dx dy |E(x, y, \xi_D)|^2 \ . \qquad \text{(III. 41)}$$

With region G evacuated, E_S is the only harmonic field at ξ_D and the signal follows from Eqs. (III. 39) and (III. 41)

$$S_0 = K|\eta X_S/\Delta k_S|^2 \ , \qquad \text{(III. 42)}$$

where $K = 2^4 \pi^4 k_0^2/c^2 A_I^2)$, (III. 43)

and A_I, a measure of the fundamental beam area at the interface, is

$$A_I = 3^{1/2} \pi b_G (1 + \xi_I^2)/2(k_0/3) \ . \qquad \text{(III. 44)}$$

Equation (III. 42) can also be deduced by using the schematic vibration curve shown in Fig. 11(c). [*Schematic* vibration curves are shown in Figs. 11(c)–11(e) since only the general shape of the curves is important to the argument.] Under the present condition that the beam area changes insignificantly within a coherence length, the curve is a tight spiral and in the region of ξ_I may be approximated by a circle. Comparison with the plane-wave vibration curve of Fig. 7(b) shows that E_S is equivalent to half the harmonic field produced by a plane wave fundamental of area A_I in one coherence length of solid. A straightforward calculation of this equivalent plane-wave case again leads to Eq. (III. 42).

The signal given by Eq. (III. 42) is unchanged if the solid S is made mildly absorbing to the harmonic radiation ($0 < \text{Im}\, \Delta k_S \ll |\Delta k_S|$) which means that there is negligible absorption within a coherence length. Mathematically this is because the approximation of Eq. (III. 38) still applies. Also the vibration curve is modified as shown in Fig. 11(d) and the argument based on it is unchanged. The harmonic field contributions originating from more than a few absorption lengths within the solid do not now reach the detector so that the extended solid region of Fig. 11(b) may be replaced by an absorbing window of sufficient thickness. This is then the experimental configuration, Fig. 11(a).

When the gas is present in region G, the harmonic field E_G generated in the gas and evaluated at ξ_D is obtained from Eqs. (III. 2), (III. 18), and (III. 31)

$$E_G(x, y, \xi_D) = (i\pi k_0^2/4k_G) b_G X_G E_0^3 \times \exp[ik_S' z_I + ik_G'(z_D - z_I)] \times \mathcal{G}(x, y, \xi_D, k_G'/b_G) \times I_G \ , \qquad \text{(III. 45)}$$

where

$$I_G = \int_{\xi_I}^{\xi_D} d\xi_G' \frac{\exp[ib_G \Delta k_G (\xi_G' - \xi_D)/2]}{(1 + i\xi_G')^2} \ . \qquad \text{(III. 46)}$$

In the limit of high gas pressure, $b_G \Delta k_G \gg 1$, I_G may be approximated by the procedure applied to I_S in Eq. (III. 38) which gives

$$I_G \approx [ib_G \Delta k_G (1 + i\xi_D)^2/2]^{-1} - \frac{\exp[i\Delta k_G b_G (\xi_I - \xi_D)/2]}{ib_G \Delta k_G (1 + i\xi_I)^2/2} \ . \qquad \text{(III. 47)}$$

The first term representing harmonic generation in the region $\xi_D < \xi' < \infty$ is made negligible by choosing ξ_D sufficiently large. Equations (III. 45) and (III. 47) then yield

$$E_G(x, y, \xi_D) = \frac{-\pi k_0}{2} \frac{X_G}{\Delta k_G} E_0{}^3 (1 + i\xi_I)^{-2} \times \exp[ik_S{}' z_I + ik_G(z_D - z_I)] \times \mathcal{G}(x, y, \xi_D, k_0/b_G) , \quad \text{(III. 48)}$$

where the refractive indices of the gas have been set to unity except in the phase and in Δk_G. The signal S_H resulting from the combination of solid and gas at high pressure is obtained from Eqs. (III. 41) and (III. 48).

$$S_H = K|\eta X_S/\Delta k_S - X_G/\Delta k_G|^2 . \quad \text{(III. 49)}$$

Inspection of vibration curves followed by a plane-wave analysis gives an alternative method leading to Eq. (III. 49) as with Eq. (III. 42). The vibration curve for the region G filled with gas at high pressure is shown in Fig. 11(e). In particular the relative phase of E_S and E_G follows directly from the vibration curves Figs. 11(d) and 11(e).

For $(X_S/\Delta k_S)$ and $(X_G/\Delta k_G)$ both real, Eqs. (III. 42) and (III. 49) yield

$$(X_G/\Delta k_G)/(\eta X_S/\Delta k_S) = 1 \pm (S_H/S_0)^{1/2} . \quad \text{(III. 50)}$$

The possibility that these quantities are complex must, however, be considered. X_G, Δk_G, and Δk_S can be assumed real with confidence since the gases used were transparent at all the frequencies involved and the imaginary part of Δk_S is finite but small. Although there is no *a priori* reason why X_S should be real, it will be shown in Sec. IV that such an assumption is in fact justified. Apart from the ambiguity arising from choice of sign, Eq. (III. 50) enables values of $(X_G/\Delta k_G)$ relative to $(\eta X_S/\Delta k_S)$ to be deduced from experimental determinations of S_H/S_0. The ambiguity of sign arises from a lack of experimental evidence for the relative phase of E_S and $(E_S + E_G)$ which would be necessary to determine whether $|X_G/\Delta k_G|$ is greater than or less than $|\eta X_S/\Delta k_S|$.

At lower gas pressures, the integral I_G of Eq. (III. 46) must be computed numerically. Computed curves for signal as a function of gas pressure are shown with experimental data in Fig. 5. Unfortunately, the shape of the curve for a given S_H/S_0 is only marginally dependent on the sign in Eq. (III. 50) and does not provide a means of resolving the ambiguity.

A few experiments were also conducted with a quartz window in place of the glass one. Quartz is transparent to the third harmonic radiation (2314 Å) and so the situation in the region G' [see Fig. 4(a)] is no longer irrelevant. When ethylene, a gas for which $(X/\Delta k)$ is close to that of quartz, was introduced on both sides of the window, results essentially according to the scheme shown in Table I were obtained. It will be seen that (iv) is an incoherent superposition of (ii) and (iii). This is because the effective thickness of the window varies by more than a coherence length depending on the ray path within the diverging beam. For obtaining quantitative results, the glass window is preferable since it leads to easily interpretable results which are independent of the window thickness.

TABLE I. Third-harmonic signal generated by a fundamental beam focused near a quartz plate separating two regions G and G' which may each be evacuated or filled with ethylene at high pressure.

	Gas pressure in G'	Gas pressure in G	Signal
i	high	high	0
ii	high	0	1
iii	0	high	1
iv	0	0	2

IV. RESULTS

Experimental Third-Harmonic Coefficients

Third-harmonic signals were measured as a function of pressure for various gases. Data for the rare gases are shown in Fig. 5. S_H was less than S_0 in all cases, indicating that

$$|(X/\Delta k)_G| < |2(\eta X/\Delta k)_S| .$$

For several gases (e.g., krypton and xenon) S_H was found to be undetectably small. This was an important result because taken together with Eq. (III. 49) and the subsequent discussion it implies that X_S is real and Eq. (III. 50) is therefore valid.

The theoretical curves shown in Fig. 5 were determined by numerical evaluation of the integral in Eq. (III. 46) and adjusted for best fit to the data. The form of these curves is expected to be essentially independent of the mode structure of the laser. The extrapolated high-pressure signal S_H was derived from the curve but is insensitive to the details of the fit. For krypton and xenon, Δk is sufficiently large so that the data points at $\frac{2}{3}$ atm are effectively at infinite pressure. Values of S_H/S_0 for each gas are shown in Table II together with alternative values (i) and (ii) for $(X/\Delta k)_G$ relative to glass. The two possibilities arise from the choice of sign in Eq. (III. 50) and correspond to $(X/\Delta k)_G$ less than or greater than $(\eta X/\Delta k)_S$, respectively. In all cases, binary

TABLE II. S_H/S_0 is the ratio of third-harmonic signals in the limits of high and low gas pressures, respectively. The value relative to glass of $(X/\Delta k)_G$, the ratio of third-harmonic coefficient to wave-vector mismatch, is derived from S_H/S_0 by use of Eq. (III.50). The ambiguity of sign in that equation yields two possible values (i) and (ii) for each gas. The data on Δk are taken from the literature and yield relative values of the third harmonic coefficient X. The convenience of the scaling employed for X will become clear in connection with Table III.

	S_H/S_0	$X/\Delta k$ relative to glass		Δk at STP	X (arbitrary units)	
		(i)	(ii)	(cm^{-1})	(i)	(ii)
He	0.30 ± 0.06	0.45 ± 0.06	1.55 ± 0.06	0.38[a]	4.0 ± 0.5	4.0 ± 0.2
Ne	0.22 ± 0.06	0.53 ± 0.06	1.47 ± 0.06	0.72[a]	8.9 ± 1.0	7.2 ± 0.4
Ar	0.05 ± 0.04	0.77 ± 0.07	1.23 ± 0.07	7.0[b]	126 ± 12	59 ± 4
Kr	< 0.02	1.00 ± 0.15	1.00 ± 0.15	16.5[c]	386 ± 57	112 ± 17
Xe	< 0.02	1.00 ± 0.15	1.00 ± 0.15	42.0[c]	979 ± 150	286 ± 43
Glass	•••	$1/\eta$	$1/\eta$	•••	•••	•••
H_2	0.18 ± 0.04	0.57 ± 0.05	1.43 ± 0.05	6.0[d]	80 ± 7	58 ± 2
CO_2	0.28 ± 0.05	0.47 ± 0.04	1.53 ± 0.04	14.2[d]	156 ± 13	147 ± 4
$(CH_2)_2$	< 0.02	1.00 ± 0.15	1.00 ± 0.15			
Cl_2	< 0.02	1.00 ± 0.15	1.00 ± 0.15			
N_2	0.24 ± 0.05	0.51 ± 0.05	1.49 ± 0.05	9.0[d]	107 ± 11	91 ± 3
O_2	0.34 ± 0.09	0.41 ± 0.08	1.59 ± 0.08			
Air	0.34 ± 0.10	0.41 ± 0.08	1.59 ± 0.08	9.0[d]	86 ± 17	97 ± 5

[a] C. Cuthbertson and M. Cuthbertson, Proc. Roy. Soc. (London) A135 40 (1932).

[b] B. Quarder, Ann. Physik 74, 255 (1924).

[c] J. Koch, Kungl. Fysiographiska Sallskapets I Lund 19, 173 (1949).

[d] International Critical Tables (National Research Council of the U.S.A.) edited by E. W. Washburn (McGraw-Hill Book Co., Inc., 1930), Vol. VII, p. 1ff.

mixtures of gases were found to yield values of S_H/S_0 intermediate between the two values for the pure gases. This reduces the possible combinations to set (i) for all gases *or* set (ii) for all gases. Table II also shows values of Δk from the literature and the corresponding two sets of relative values for the third-harmonic coefficients X which are scaled for convenience in connection with Table III. It will be shown later that set (i) is in substantial agreement with other data.

$(X/\Delta k)$ was shown in Sec. III to be the important parameter governing harmonic generation under nonindex-matched conditions. $(X/\Delta k)$ is independent of density and the experimental results of Table II show that it is also essentially independent of the material. For the rare gases, for instance, whereas the coefficient X varies over two orders of magnitude, $(X/\Delta k)$ is constant to within a factor $\times 2$. This can be understood on the basis of perturbation theory (see Appendix C).

The absolute value of $|\eta X/\Delta k|$ for glass was estimated from measurements of S_0 by using Eqs. (III.42) and (III.43), and was then employed to derive an absolute third-harmonic coefficient for each gas from the relative values given in Table III. However, a much larger uncertainty must be associated with the absolute coefficients. Additional parameters involved in the determination of $(\eta X/\Delta k)$ for glass are (with corresponding uncertainties in parentheses): The absolute laser power which was measured in terms of optical rectification in ammonium dihydrogen phosphate using the known value of the optical rectification coefficient[11a]

$$[X_{xyz}(0;\omega,-\omega)+X_{xzy}(0;\omega,-\omega)]$$

($\pm 15\%$), the beam area at the glass window A_I which was estimated by burning exposed Polaroid film ($\times 2^{\pm 1}$), transmission at 2314 Å from the gas cell to photomultiplier including the $NiSO_4$ filter ($\pm 15\%$), the quantum efficiency of the photomultiplier taken from the manufacturer's specification ($\pm 25\%$) and the gain of the photomultiplier and electronics which was determined from a statistical analysis of single photon signals ($\pm 10\%$). Also the coefficient derived from Eqs. (III.42) must be divided by a factor $\sqrt{\mu}$ unless the laser beam is a single lowest-order Gaussian mode. μ increases to six if many confocal lowest-order modes are present and would also be increased by mode locking and the presence of higher-order modes. A crude assessment of the mode structure for our laser leads to the assignment $\sqrt{\mu} = 2 \pm 1$. The absolute results which are uncertain to within a factor of 3 are

$$(\eta X/\Delta k)_{\text{glass}} = 1.1 \times 10^{-18} \text{ esu}, \qquad \text{(IV.1)}$$

which yields for helium

$$(X/\Delta k)_{\text{He}} = 5 \times 10^{-19} \text{ esu (i)}$$

TABLE III. Comparison of nonlinear coefficients in units of 10^{-39} esu/atom. Two sets of experimental third-harmonic coefficients χ corresponding to the ambiguity in sign of Eq. (III.50) are compared with other data. "χ theoretical" are the results of direct calculations. "χ derived" are derived from the Kerr coefficient χ^K or dc hyperpolarizability χ^0 shown to their right using Eq. (IV.4) with the effective excitation energy ω_n. All values are absolute *except* those in columns two–four for gases other than helium where the values are normalized to χHe$=4.0\times10^{-39}$ esu/atom. The absolute experimental third-harmonic coefficients for helium have been refined and reduced by 30% since publication in Ref. 3.

	χ experimental (i)	χ experimental (ii)	χ theoretical	χ derived	ω_n (10^3 cm^{-1})	χ^K	χ^0 theoretical
	absolute						
He	$7.0\times3^{\pm1}$	$24\times3^{\pm1}$	4.0[a]				
			12.0[b]				
			0.9[c]				
				3.88	170	3.66[a]	
				3.87			3.58[a]
				3.88			3.59[d]
				4.9		4.5 ± 0.3[e]	
	relative to $\chi_{He}=4.0$						
Ne	8.9 ± 1.5	7.2 ± 0.5	7.6[c]	9.8	130	8.5 ± 0.7[e]	
				12.0			10.4[d]
Ar	126 ± 20	59 ± 5	124[c]	127	93	98 ± 7[e]	
				250			194[d]
Kr	386 ± 75	112 ± 25	316[c]	317	80	233 ± 17[e]	
Xe	979 ± 190	286 ± 45	987[b]	962	67	650 ± 50[e]	
H_2	80 ± 12	58 ± 4		61[f]		47 ± 5[f]	
CO_2	156 ± 23	147 ± 8					
N_2	107 ± 17	91 ± 5					

[a] P. Sitz and R. Yaris, J. Chem. Phys. 49, 3546 (1968).
[b] See Appendix B.
[c] E. L. Dawes, Phys. Rev. 169, 47 (1968).
[d] P. W. Langhoff, J. D. Lyons, and R. P. Hurst, Phys. Rev. 148, 18 (1966); M. N. Grasso, K. T. Chung, and R. P. Hurst, *ibid.* 167, 1 (1968).
[e] A. D. Buckingham and D. A. Dunmur, Trans. Faraday Soc. 64, 1776 (1968).
[f] A. D. Buckingham and B. J. Orr, Proc. Roy. Soc. (London) A305, 259 (1968).

or 17×10^{-19} esu (ii) . (IV.2)

Microscopic coefficients χ are obtained by dividing X by the number density of atoms or molecules [see Eq. (A.11) and discussion]. The result for helium is

$$\chi_{He} = 7\times10^{-39} \text{ esu/atom (i)}$$

or 24×10^{-39} esu/atom (ii) . (IV.3)

In the case of molecules χ obtained in this way represents an average over spatial orientations.

Comparison of Third-Harmonic Coefficients with Other Data

Experimental third-harmonic coefficients are assembled in Table III with other data from the literature for comparison.

Three directly calculated values for X_{He} are given in column four: The first is the result of a time-dependent perturbation variation calibration by Sitz and Yaris[12] which is though to be good to about 1%. It is, however, unlikely that the method can be profitably extended to other atoms.[13] The second comes from a time-dependent perturbation calculation (see Appendix B) which could be extended to those other atoms where a considerable amount of information on matrix elements is available. The estimated uncertainty is large enough so that no significicance is to be attached to the difference (a factor of 3) between this result and that of Sitz and Yaris. The third is a calculation by Dawes[14] using a perturbation approach where the sum over intermediate states is reduced to a single effective term and linear polarizabilities are used as input data. This calculation is readily

extendable to other atoms. Again the estimated uncertainty is large enough so that no significance is to be attached to the difference (a factor of 4) between this result and that of Sitz and Yaris.[15] The absolute experimental values for X_{He} have large uncertainties ($\times 3^{\pm 1}$) but (i) exhibits substantially better agreement with theory than (ii).

χ can also be inferred from the Kerr coefficient χ^K and from the dc hyperpolarizability χ^0. These coefficients are here so defined (see Appendix A) that they are equal if the frequency ω_1 of the applied optical field is negligible compared with frequencies ω_n characteristic of the atom. For ω_1/ω_n small but not negligible, the ratio of the coefficients estimated from time-dependent perturbation theory is

$$\chi^0 \approx \chi^K/(1+5\omega_1^2/[2\omega_n^2]) \approx \chi/(1+15\omega_1^2/\omega_n^2), \tag{IV.4}$$

where ω_n is an effective characteristic frequency assigned by inspection of the term scheme. Column five of Table III contains values for χ derived from χ^0 or χ^K using Eq. (IV.4). In particular, theoretical values calculated by Sitz and Yaris[12] for helium are processed in this way and may be compared with their directly calculated χ_{He} as a check on the procedure. Experimental values for χ^K measured by Buckingham and Dunmur[16] and recent theoretical values for χ^0 are also given in Table III and used with Eq. (IV.4) to estimate values for χ. These values of χ^0 are the results of variational calculations by Hurst and co-workers.[17] For helium the result, which is thought to be good to about 1%, is in excellent agreement with the value calculated by Sitz and Yaris.

The ratio of experimental third-harmonic coeffi cients for different gases is known much more precisely (about 20%) than the absolute values ($\times 3^{\pm 1}$). To make use of this, the experimental χ shown in Table III for gases other than helium are scaled to $X_{He} = 4.0 \times 10^{-39}$ esu/atom – the Sitz and Yaris value. (Dawes theoretical values are similarly normalized.) It can be seen that set (i) is in broad agreement with the other data but set (ii) is not. We conclude set (i) represents the correct resolution of the ambiguity in Eq. (III.50) and that $|X/\Delta k|$ for these gases is less than $|\eta X/\Delta k|_{glass}$.

V. CONCLUSION

The theory of third harmonic generation by focused beams in homogeneous media has been discussed and used to extract third-harmonic coefficients from measurements on various gases. Absolute uncertainties are large ($\times 3^{\pm 1}$) but ratios are good to about 20%. An ambiguity leads to two sets of third-harmonic coefficients, one of which is spurious. Set (i) is found to be in good agreement with a broad range of data on nonlinear coefficients.

ACKNOWLEDGMENTS

It is a pleasure to acknowledge helpful conversations with E. L. Dawes, M. V. Hobden, P. A. Franken, R. Yaris, and B. J. Orr.

APPENDIX A: DEFINITIONS OF NONLINEAR COEFFICIENTS

Various definitions of nonlinear coefficients are used in the literature. That used in this paper is reviewed here.

The applied electric field $\vec{E}(\vec{r}, t)$ in the medium is

$$\vec{E}(\vec{r}, t) = \vec{E}^0(\vec{r}) + \sum_i \tfrac{1}{2}[\vec{E}^{\omega i}(\vec{r})e^{-i\omega_i t} + \vec{E}^{\omega i *}(\vec{r})e^{+i\omega_i t}], \tag{A.1}$$

where $$\vec{E}^{\omega i *}(\vec{r}) = \vec{E}^{-\omega i}(\vec{r}). \tag{A.2}$$

The resulting polarization is

$$\vec{P}(\vec{r}, t) = \vec{P}^0(\vec{r}) + \sum_\sigma \tfrac{1}{2}[\vec{P}^{\omega\sigma}(\vec{r})e^{-i\omega_\sigma t} + \vec{P}^{\omega\sigma *}(\vec{r})e^{+i\omega_\sigma t}], \tag{A.3}$$

where $$\vec{P}^{\omega\sigma *}(\vec{r}) = \vec{P}^{-\omega\sigma}(\vec{r}). \tag{A.4}$$

The nonlinear tensor susceptibilities $\underline{X}$ are defined by

$$\vec{P}^{\omega\sigma}(\vec{r}) = K(-\omega_\sigma; \omega_1, \omega_2 \cdots) \times \underline{X}(-\omega_\sigma; \omega_1, \omega_2 \cdots)\vec{E}^{\omega_1}(\vec{r}) \times E^{\omega_2}(\vec{r}) \times \cdots \tag{A.5}$$

$\underline{X}^*(-\omega_\sigma; \omega_1, \omega_2 \cdots)$ is defined by the complex-conjugate equation to Eq. (A.5) but the coefficient is expected to be real unless resonant processes involving damping are important. The frequency labels satisfy the relation

$$\omega_\sigma = \omega_1 + \omega_2 + \cdots. \tag{A.6}$$

$K(-\omega_\sigma; \omega_1, \omega_2 \cdots)$ is a real function of its frequency labels only and is of order unity. It is defined so that

$$K(0; 0, 0 \cdots) = 1, \tag{A.7}$$

and so that for all processes of a particular order

(involving a particular number of applied fields), $\underline{X}(-\omega_\sigma;\omega_1,\omega_2\cdots)$ approaches $\underline{X}(0;0,0\cdots)$ as all the frequencies tend to zero. This is especially convenient for the intercomparison of various processes of a particular order. The values of K for processes of interest here are

$$\begin{aligned} K(0;0,0,0) &= 1 \quad \text{dc hyperpolarizability}\\ K(-3\omega;\omega,\omega,\omega) &= \tfrac{1}{4} \quad \text{third harmonic generation}\\ K(-\omega;\omega,0,0) &= 3 \quad \text{Kerr effect}\\ K(-2\omega;\omega,\omega) &= \tfrac{1}{2} \quad \text{second harmonic generation.} \end{aligned} \tag{A.8}$$

The order of the field frequency labels $\omega_1,\omega_2\cdots$ in $\underline{X}(\omega_\sigma;\omega_1,\omega_2\cdots)$ is taken to be irrelevant: All processes obtained by permuting $\omega_1,\omega_2\cdots$ are included in $\underline{X}(-\omega_\sigma;\omega_1\omega_2\cdots)$.

The symmetry of an isotropic medium restricts a fourth rank tensor to 21 nonzero elements, three of which are independent. For third harmonic generation there is only one independent element, say X_{zzzz}, where

$$X_{zzzz}=X_{iiii}=(X_{iijj}+X_{ijij}+X_{ijji})\ ;\quad i,j=x,y,z;\quad i\neq j \tag{A.9}$$

The microscopic nonlinear polarizability $\underline{\chi}$ is related to $\underline{X}$ by[18]

$$\underline{X}(-\omega_\sigma;\omega_1,\omega_2\cdots) = N[L(\omega_\sigma)\times L(\omega_1)\times L(\omega_2)\times\cdots]\times\underline{\chi}(-\omega_\sigma;\omega_1,\omega_2\cdots)\ , \tag{A.10}$$

where N is the number density of microscopic systems and $L(\omega)$ is the ratio of local to applied field at frequency ω. For all gases discussed here at pressures of less than 10 atm we set all $L(\omega)$ to unity so that

$$\underline{X}=N\underline{\chi}\ . \tag{A.11}$$

While the processes are not directly comparable in this respect we do not expect deviations from a linear dependence of $\underline{X}$ on pressure greater than those observed for the Kerr effect which are insignificant at the pressures used here.

In the literature of physical chemistry a coefficient γ is used to describe third-order processes where

$$\underline{X}(-\omega_\sigma;\omega_1,\omega_2,\omega_3)=\tfrac{1}{6}\underline{\gamma}(-\omega_\sigma;\omega_1,\omega_2,\omega_3)\ . \tag{A.12}$$

The factor $\frac{1}{6}$ arises from expanding the energy of the system as a Taylor series in the electric field.

In the body of this paper abbreviated notations for coefficients are used where convenient

$$\begin{aligned} X^{(q)} &= X(-q\omega;\omega,\omega\ldots),\\ X &= (-3\omega;\omega,\omega,\omega),\\ \chi &= \chi(-3\omega;\omega,\omega,\omega),\\ \chi^0 &= \chi(0;0,0,0),\\ \chi^K &= \chi(-\omega;\omega,0,0)\ . \end{aligned} \tag{A.13}$$

Coordinate subscripts $zzzz$ are omitted and a subscript is sometimes used to identify the nonlinear medium.

APPENDIX B. TIME-DEPENDENT PERTURBATION CALCULATION OF THE THIRD-HARMONIC COEFFICIENT FOR HELIUM

We have made a calculation of the third-harmonic coefficient for a helium atom using standard time-dependent perturbation theory:

$$\begin{aligned} \chi_{zzzz}(-3\omega;\omega,\omega,\omega) &= (e^4/\hbar^3)\sum_n\sum_m\sum_{n'}\\ &\times\langle g|z|n\rangle\langle n|z|m\rangle\langle m|z|n'\rangle\langle n'|z|g\rangle\\ &\times\{[(\omega_n-3\omega)(\omega_m-2\omega)(\omega_{n'}-\omega)]^{-1}\\ &+[(\omega_n+\omega)(\omega_m+2\omega)(\omega_{n'}+3\omega)]^{-1}\\ &+[(\omega_n+\omega)(\omega_m-2\omega)(\omega_{n'}-\omega)]^{-1}\\ &+[(\omega_n+\omega)(\omega_m+2\omega)(\omega_{n'}-\omega)]^{-1}\}\ . \end{aligned} \tag{B.1}$$

For comparison, the linear optical polarizability, related to the refractive index is

$$\chi_{zz}(-\omega;\omega)=(e^2/\hbar)\sum_n\langle g|z|n\rangle\langle n|z|g\rangle\times[(\omega_n-\omega)^{-1}+(\omega_n+\omega)^{-1}]\ . \tag{B.2}$$

In these expressions $\langle g|z|n\rangle$ is a matrix element of z between the ground state g and an excited state n at energy $\hbar\omega_n$. The sums are over all intermediate states including singly excited states, doubly excited states and the continuum. Terms where $m=g$ also contribute.

$\chi_{zz}(-\omega;\omega)$ has been computed by Vinti[19] and it is useful to compare that problem with the calculation of $\chi_{zzzz}(-3\omega;\omega,\omega,\omega)$.

(i) $\chi_{zz}(-\omega;\omega)$: involves a single (infinite) sum; requires only $1S$-nP matrix elements; These matrix elements enter as the modulus squared so that no knowledge of the sign of the matrix element is necessary and all contributions have the same sign (for $\omega<\omega_{1P}$).

(ii) $\chi_{zzzz}(-3\omega;\omega,\omega,\omega)$: involves a triple infinite sum; requires all $nP-mS$, $nP-mD$ matrix elements; the signs of matrix elements are important and significant cancellation occurs between various terms in the sum.

Thus the nonlinear coefficient requires more data and is more sensitive to its accuracy than is the linear coefficient. Also, Vinti showed that for helium the dominant contribution to $\chi_{zz}(-\omega;\omega)$ was from the continuum. The same is not necessarily true for $\chi_{zzzz}(-3\omega;\omega,\omega,\omega)$. In any case we ignore both the continuum and doubly excited states and calculate the contribution due to singly excited states only. Matrix elements were derived from the following sources in order of preference:

(a) Magnitude from measured absorption f numbers and sign from method b.

(b) Coulomb approximation calculations of Bates and Damgaard.[20]

(c) Extrapolation from the table of Bates and Damgaard.

(d) Interpolation within the array of matrix elements.

All terms in the triple sum were included which contained no P states higher than $11P$ nor any S state higher than $9S$ nor any D state higher than $7D$. On the basis of the rate of convergence it is estimated that the total contribution involving higher discrete states is small.

The result is that for helium with $2\pi c/\omega = 6943$ Å

$$\chi_{zzzz}(-3\omega;\omega,\omega,\omega) = 12\times10^{-39} \text{ esu/atom} . \quad \text{(B.3)}$$

No account has been taken of the continuum.

APPENDIX C. VARIATION OF X AND $X/\Delta k$ FROM GAS TO GAS

Multiplying the expression for $\chi(-3\omega_1;\omega_1,\omega_1,\omega_1)$ calculated from perturbation theory [Eq. (B.1)] by N, the number density of atoms, gives the corresponding expression for $X(-3w_1;w_1,w_1,w_1)$ [see Eq. (A.11)]. The mismatch parameter Δk is related to $\chi(-\omega;\omega)$ given in Eq. (B.2) by

$$\Delta k = [12\pi\omega_1 N/c(n_1+n_3)][\chi(-3\omega_1;3\omega_1)-\chi(-\omega_1;\omega_1)] , \quad \text{(C.1)}$$

where the refractive indices n_1 and n_3 may be set equal to unity for a gas. If the sum in Eq. (B.2) is replaced by a single effective term, the form of the result is

$$\chi(-\omega;\omega) = \text{constants}\times(\text{matrix elements}) \times[(\omega_n+\omega)^{-1}+(\omega_n-\omega)^{-1}] . \quad \text{(C.2)}$$

Equation (C.2) gives a good fit to refractive-index data for many gases when "matrix elements" and ω_n are treated as a pair of free parameters for each gas. Similarly reducing the sums in $\chi(-3\omega_1;\omega_1,\omega_1,\omega_1)$ and

$$[\chi(-3\omega_1;3\omega_1)-\chi(-\omega_1;\omega_1)]$$

to single effective terms and using the approximation $\omega_1^2/\omega_n^2 \ll 1$ leads to expressions of the form

$$X(-3\omega_1;\omega_1,\omega_1,\omega_1) = \text{constants}\times(\text{matrix elements})\times(\omega_n^{-3}+\cdots) \quad \text{(C.3)}$$

and

$$\Delta k \propto [\chi(-3\omega_1;3\omega_1)-\chi(-\omega_1;\omega_1] = \text{constants}\times(\text{matrix elements}\times(\omega^3/\omega_n^3+\cdots) \quad \text{(C.4)}$$

Thus whereas the third-harmonic coefficient X is strongly dependent on ω_n and matrix elements, the ratio $X/\Delta k$ is independent of ω_n and is less dependent on matrix elements. It is therefore to be expected that the variation from gas to gas of X will be more marked than that of $X/\Delta k$. The experimental results of Table II demonstrate this feature.

---

*Work supported in part by the U. S. Atomic Energy Commission. The experimental part of the program was carried out at the Clarendon Laboratory, University of Oxford, Oxford, England and this paper is based on a thesis submitted by one of us (G. H. C. N.) in partial fulfillment of the requirements for the degree of Ph. D. in Physics at the University of Oxford.

[1]P. A. Franken, A. E. Hill, C. W. Peters, and G. Weinreich, Phys. Rev. Letters 7, 118 (1961).

[2]P. D. Maker, R. W. Terhune, and C. M. Savage, in Proceedings of the Third International Conference on Quantum Electronics, Paris, 1963, edited by P. Grivet and N. Bloembergen (Columbia University Press, New York, 1964), p. 1559; P. D. Maker and R. W. Terhune, Phys. Rev. 137, A801 (1965).

[3]G. H. C. New and J. F. Ward, Phys. Rev. Letters 19, 556 (1967).

[4]P. P. Bey, J. F. Guiliani, and H. Rabin, Phys. Letters 26A, 128 (1968).

[5]J. E. Bjorkholm, Phys. Rev. 142, 126 (1966).

[6]D. A. Kleinman, A. Ashkin, and G. D. Boyd, Phys. Rev. 145, 338 (1966).

[7]D. A. Kleinman and R. C. Miller, Phys. Rev. 148, 302 (1966).

[8]D. A. Kleinman, Phys. Rev. 128, 1761 (1962).

[9]Vibration curves are commonly used in graphical treatments of diffraction [see, for example, F. A. Jenkins and H. E. White, Fundamentals of Optics

(McGraw-Hill Book Co., Inc., New York, 1957), 3rd ed., p. 295 ff], where each infinitesimal vector represents the contribution to the diffracted field due to an element of area of the diffracting aperture.

[10]The possibility of applying vibration curves to the present problem was first suggested by M. V. Hobden (private communication).

[11]Subscripts *I* and *D* are used to indicate the solid/gas interface and the plane of the detector, respectively. Also, subscripts *G* and *S* will be used to refer to regions occupied by gas and solid, respectively. There should be no confusion with the integral *I* or one signal *S*.

[11a]J. F. Ward, Phys. Rev. 143, 569 (1966).

[12]P. Sitz and R. Yaris, J. Chem. Phys. 49, 3546 (1968).

[13]R. Yaris (private communication).

[14]E. L. Dawes, Phys. Rev. 169, 47 (1968).

[15]E. L. Dawes (private communication).

[16]A. D. Buckingham and D. A. Dunmur, Trans. Faraday Soc. 64, 1776 (1968).

[17]P. W. Langhoff, J. D. Lyons, and R. P. Hurst, Phys. Rev. 148, 18 (1966); M. N. Grasso, K. T. Chung, and R. P. Hurst, *ibid.* 167, 1 (1968).

[18]J. A. Armstrong, N. Bloembergen, J. Ducuing, and P. S. Pershan, Phys. Rev. 127, 1918 (1962).

[19]J. P. Vinti, Phys. Rev. 42, 632 (1932); 44, 524 (1933).

[20]D. R. Bates and A. Damgaard, Phil. Trans. Roy. Soc. London Ser. A 242, 101 (1949).

PHYSICAL REVIEW VOLUME 185, NUMBER 1 5 SEPTEMBER 1969

High-Energy Bremsstrahlung in Collisions of Electrons with One- and Two-Electron Atoms

Robert J. Gould
School of Physics, University of Sydney, Sydney, Australia 2006
and
Department of Physics, University of California, San Diego, California 92037*

(Received 3 February 1969)

A brief discussion of the fundamental formulas for electron-electron and electron-atom bremsstrahlung is given. Some general results are given for complex atoms and explicit expressions for the cross sections for one- and two-electron atoms are exhibited graphically. It is shown that for 1*e* and 2*e* atoms which have a residual charge, that is, for ions, the total cross section is composed of several terms, one of which is $(Z-1)^2$ or $(Z-2)^2$ (respectively) times the cross section for electrons incident on unshielded protons. Some results for general atoms or molecules in the high- and low-energy limits are indicated.

I. INTRODUCTION

Bremsstrahlung in encounters of high-energy charged particles is an old problem, first treated in detail by Bethe and Heitler[1] and by Bethe.[2] It is closely associated with the process of pair production which has essentially the same set of Feynman diagrams and corresponding matrix elements. While the problem of bremsstrahlung (and pair production) in a pure unshielded static Coulomb field is regarded to have been solved satisfactorily in the original work of Bethe and Heitler, some confusion has continued to exist regarding electron-electron bremsstrahlung. Basically, the question is whether, in the latter, recoil and exchange effects come in; we shall return to this point shortly. These questions are relevant not only to the problem of bremsstralung in the scattering of two free electrons, but also to the case where one electron is (initially, at least) bound in an atom. For low-Z atoms especially, it is important to treat accurately the effects of the interaction of the incoming high-energy electron with the atomic electrons. The total bremsstrahlung cross section for an electron incident on an atom or ion is essentially proportional to $Z^2 + Z_{el}$, where Z is the nuclear charge and Z_{el} is the number of atomic electrons. Moreover, as Wheeler and Lamb[3] have emphasized, it is necessary to sum over final states (including the continuum) of the atomic system which scatters the incoming electron. Actually the dependence ($\propto Z^2 + Z_{el}$) of the total cross section on nuclear charge and number of atomic electrons appears only after this summation over final states is performed.

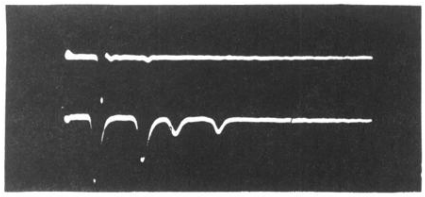

FIG. 2. Double-beam oscilloscope trace of third-harmonic (upper) and fundamental monitor (lower) signals. The cubic dependence of $\mathcal{P}^{3\omega 1}$ on $\mathcal{P}^{\omega 1}$ not only affects the relative pulse heights in each channel but also causes the harmonic pulses to be narrower than the fundamental pulses.